Exploring the large-scale structure of Taylor–Couette turbulence through Large-Eddy Simulations

IOP Conf. Series: Journal of Physics: Conf. Series **1001** (2018) 012017 doi:10.1088/1742-6596/1001/1/012017

Exploring the large-scale structure of Taylor–Couette turbulence through Large-Eddy Simulations

Rodolfo Ostilla-Mónico[1,2], Xiaojue Zhu[3], Roberto Verzicco[3,4]

[1] School of Engineering and Applied Sciences, Harvard U., Cambridge, MA 02138, USA.
[2] Dept. of Mechanical Engineering, U. of Houston, Houston, Texas 77204, USA.
[3] Physics of Fluids Group, Faculty of Science and Technology, MESA+ Research Institute, and J. M. Burgers Centre for Fluid Dynamics, U. Twente, PO Box 217, 7500 AE Enschede, The Netherlands.
[4] Dipart. Ing. Industriale, U. Rome "Tor Vergata", Via del Politecnico 1, Roma 00133, Italy

E-mail: rostilla@central.uh.edu

Abstract. Large eddy simulations (LES) of Taylor-Couette (TC) flow, the flow between two co-axial and independently rotating cylinders are performed in an attempt to explore the large-scale axially-pinned structures seen in experiments and simulations. Both static and dynamic LES models are used. The Reynolds number is kept fixed at $Re = 3.4 \cdot 10^4$, and the radius ratio $\eta = r_i/r_o$ is set to $\eta = 0.909$, limiting the effects of curvature and resulting in frictional Reynolds numbers of around $Re_\tau \approx 500$. Four rotation ratios from $Rot = -0.0909$ to $Rot = 0.3$ are simulated. First, the LES of TC is benchmarked for different rotation ratios. Both the Smagorinsky model with a constant of $c_s = 0.1$ and the dynamic model are found to produce reasonable results for no mean rotation and cyclonic rotation, but deviations increase for increasing rotation. This is attributed to the increasing anisotropic character of the fluctuations. Second, "over-damped" LES, i.e. LES with a large Smagorinsky constant is performed and is shown to reproduce some features of the large-scale structures, even when the near-wall region is not adequately modeled. This shows the potential for using over-damped LES for fast explorations of the parameter space where large-scale structures are found.

1. Introduction

Numerical simulation is a powerful tool for turbulence research because it provides us with the ability to reproduce virtually any quantity, including those which are unavailable in experiments. Direct numerical simulation (DNS) is certainly the best choice from a modeling perspective as it solves all the flow scales up to the smallest scale. However, DNS is computationally very expensive at high Reynolds number which prohibits simulations of practical applications of turbulence. Large eddy simulation (LES) is a less expensive alternative in which the fundamental idea is to reduce the computational cost by using a coarser discretization, and accounting for the small eddies, which are not resolved, by a subgrid-scale (SGS) model. In the last two decades, LES has been successfully implemented in many paradigmatic wall-bounded turbulent flows, such as channel flow [1], pipe flow [2] and boundary layer flow [3]. For additional information on the general topic of LES, we refer the readers to the book by Sagaut [4] or the review by Meneveau and Katz [5].

Here we focus on another paradigmatic flow, Taylor-Couette (TC) flow. TC flow is the flow between two co-axial and independently rotating cylinders, and it has attracted a lot of

attention in recent years [6]. It is a popular toolbox for the new development of concepts in fluid dynamics, from instabilities, nonlinear dynamics, pattern formation- and turbulence, the subject of the present study. There are two distinct differences between TC turbulence and the previously mentioned paradigmatic wall-bounded flows: the first is the curvature of the walls and the second is the presence of a considerable mean rotation imposed on the mean shear flow. It is expected that these two effects will have huge impacts on the turbulence properties.

TC turbulence can be used as a benchmark for LES as it has two opposing curvatures, convex and concave at both cylinders, and also the amount of mean rotation can be easily varied using the differential rotation of the cylinders. Due to the high amount of symmetries, and natural confinement, TC is easily realized experimentally up to high Reynolds numbers: velocity profiles have been measured up to $Re \sim \mathcal{O}(10^6)$ [7], so we are not limited by the Reynolds numbers we can reach in experiments for validation.

In TC turbulence, persistent and spatially stable large scale known as turbulent Taylor vortices or Taylor rolls are known to exist. Understanding their origin is very important as it is one of the key mechanisms by which angular velocity is transported in TC flow [8, 9]. Recently, in turbulent channel and Couette flows, Hwang & Cossu [10, 11] showed that large-scale motions can exist even in the absence of small scales of turbulence. This was done by a method known as over-damped LES, which consists of using an LES filter without energy backscatter and artificially increasing its dissipation characteristics. In this way, the small scale motions are suppressed while the dissipation associated to them is kept.

However, different from pipe, channel or Couette flows, where large-scale motions contain only a significant amount of energy for sufficiently high Reynolds number [12], in TC turbulence the turbulent Taylor vortices are suspected to be simply a continuation of the laminar Taylor rolls, i.e. low Reynolds number structures originating from centrifugal instability. Therefore over-damped LES should always show these motions regardless of Reynolds number. Nevertheless, even at low Reynolds numbers Taylor rolls show substantial azimuthal modulation before the transition to chaos [13]. Overdamped LES can then help us elucidate if long-wavelength azimuthal modulations of the turbulent Taylor rolls exist, for which indications were found in Ref. [14].

In this study, we set out with two goals. First, we attempt to validate reference cases for LES with static Smagorinsky and dynamic SGS models in TC turbulence to test whether LES can work in the conditions of wall curvature and mean rotation. This sets a basis for the second step, namely performing simulations of overdamped LES, focusing on the modulations of turbulent Taylor vortices.

2. Numerical details

A second-order, centered finite difference code is used to solve the incompressible Navier-Stokes equations in cylindrical coordinates [15]. The resulting discretized system is solved by a fractional-step method: the time advancement is realized through a hybrid low-storage third-order Runge-Kutta approach. The convective terms are discretized by the second-order-explicit Adams-Bashforth scheme and the viscous terms are discretized by the second-order-implicit Crank-Nicholson scheme. One-dimensional MPI directives are adopted for parallelization, i.e. what is commonly known as a slab decomposition. In recent years, the code has been extensively validated and used for the DNS of TC turbulence [8, 16].

As stated before, two SGS models are implemented for LES. First, we use the static Smagorinsky model, including a van Driest damping function,

$$\nu_t = (c_s\Delta)^2 D(r^+)|\mathcal{S}| = (c_s\Delta)^2 D(r^+)\sqrt{2S_{ij}S_{ij}} \tag{1}$$

with $S_{ij} = \frac{1}{2}\left(\frac{\partial u_i}{\partial x_j} + \frac{\partial u_j}{\partial x_i}\right)$ the resolved-scale strain rate tensor, the "filter" length scale Δ is

calculated as $\Delta = (\Delta x_1 \Delta x_2 \Delta x_3)^{1/3}$, where Δx_i is the grid width in the $i-$direction and c_s is the Smagorinsky constant. The van Driest damping function D is defined as

$$D(r^+) = 1 - \exp(r^+/25)^\alpha, \tag{2}$$

where r^+ is the wall-distance in viscous (inner) units, and $\alpha = 3$ controls the asymptotic behaviour close to the wall. As the asymptotic near-wall behaviour of the mixing length has been hypothesized to behave differently in TC flow [17], we simulate selected cases using an alternative van Driest model, denoted by D', which uses $\alpha = 2$.

For additional benchmarking, we use the dynamic LES model [18] to control the possible effects not captured by the static model. The dynamic model has been used successfully by Piomelli *et al.* [19] to simulate rotating channel flow, and has been shown to overcome some of the shortcomings of the static model, which we will discuss later. For numerical stability, we average the resulting (space- and time-dependent) C_s in the azimuthal coordinate.

The geometry considered is a Taylor-Couette system with a radius ratio $\eta = r_i/r_o$ of $\eta = 0.909$, where r_i (r_o) is the inner (outer) cylinder radius. This value of η limits the effects of curvature. Axially periodic boundary conditions, with a non-dimensional period of $\Gamma = L_z/(r_o - r_i) = 4.66$ are used. This is large enough to fit two Taylor roll pairs. A rotational symmetry order 10 is imposed on the flow, which results in a streamwise (azimuthal) extent of the domain of 2π gaps at the inner cylinder. A convective reference frame is used, such that the velocities of both cylinders are $\pm U/2$, separating differential rotation (shear) from mean rotation. The shear Reynolds number $Re_s = U(r_o - r_i)/\nu$, with ν the kinematic viscosity is fixed as $Re_s = 3.56 \cdot 10^4$. Four rotation numbers $Rot = 2\Omega_{rf}(r_o - r_i)/U$, with Ω_{rf} the rotation rate of the reference frame, are simulated: $Rot = 0$ (no mean rotation), $Rot = 0.0909$ (pure inner cylinder rotation), $Rot = 0.3$ (co-rotating cylinders) and $Rot = -0.0909$ (strongly counter-rotating cylinders) We note that positive values of Rot denote *co*-rotating cylinders which have *anti*-cyclonic mean rotation, while counter-rotating cylinders correspond to cyclonic rotation, and that the rotation number is simply the inverse of the Rossby number $Rot = 1/Ro$.

These parameters result in frictional Reynolds numbers $Re_\tau = u_\tau(r_o - r_i)/(2\nu)$ of $Re_\tau \approx 500$, where u_τ is the frictional velocity $u_\tau = \sqrt{\tau_w/\rho}$, τ_w the mean shear at the wall and ρ the fluid density. The shear at the outer cylinder has a geometrical factor η with respect to the inner cylinder normalizations, neglected unless otherwise mentioned. The viscous length δ_ν is defined as $\delta_\nu = \nu/u_\tau$. For convenience we also define the "outer" normalized radius $\tilde{r} = (r - r_i)/(r_o - r_i)$. The LES resolutions used are $N_\theta \times N_r \times N_z = 256 \times 128 \times 288$, which in viscous units correspond to $r_i \Delta\theta^+ \approx 24.5$, $\Delta r^+ \in (0.9, 11.0)$ and $\Delta z^+ \approx 16$. These resolutions are approximately twice as fine as the resolutions of Hwang & Cossu [10] (validated by Härtel and Kleiser [20]), as we use finite differences, in place of spectral methods.

Using the static model, we run a series of cases with $c_s \in [0, 0.6]$, going from $c_s = 0$ which switches off the SGS model, and is used for benchmarking purposes, to artificially high values of c_s. These are benchmarked against well-resolved DNS reference cases, which have half the domain size of the LES simulations in both streamwise and axial directions. This does not considerably affect mean and r.m.s. statistics [21]. The reference cases have resolutions of $N_\theta \times N_r \times N_z = 384 \times 512 \times 768$, which in non-dimensional terms is $r_i \Delta\theta^+ \approx 8.2$, $\Delta r^+ \in (0.2, 2.9)$ and $\Delta z^+ \approx 3$. Statistics for all simulations are collected until the radial flux of angular momentum $J^\omega = r^3(\langle u_r \omega \rangle_{t,\theta,z} - \nu \partial_r \langle \omega \rangle_{t,\theta,z})$ is constant within one percent, where $\langle ... \rangle_i$ denotes averaging with respect to variable i. The radial flux of angular momentum (torque at the cylinders) is non-dimensionalized as a quasi-Nusselt number $Nu_\omega = J^\omega / J^\omega_{pa}$ where J^ω_{pa} is the angular current for the laminar, purely azimuthal flow, $J^\omega_{pa} = (2\nu r_i^2 r_o^2 [\omega_i - \omega_o])/(r_o^2 - r_i^2)$.

3. LES of Taylor-Couette flow with no mean rotation

First, we focus on TC flow with no mean rotation, i.e. $Rot = 0$. Table 1 shows Nu_ω for the different cases ran, both LES with the static and dynamic models, as well as the reference cases. The under-resolved reference case ($c_s = 0$) overestimates the torque. Increasing c_s activates the SGS models and the torque decreases. This can be reasoned by noting that increasing c_s increases the turbulent viscosity (stress), and as the stresses increase, the strains decrease as the LES model self-adjusts [22]. And as a consequence of the deceased strains, a lower torque results.

For the static model with $c_s = 0.1$ a good agreement is achieved with the reference data, regardless of the van Driest model used. The simulations with a static c_s larger than 0.2, correspond to "overdamped" LES. These show torques which are more than 10% under the reference value. For $c_s \geq 0.4$, the underlying small-scale flows are almost completely the damped, and Nu_ω shows a drastic decrease for $c_s = 0.6$. These cases will be discussed in Section 5, for the time being, we focus on cases ran with conventional values of c_s and use the simulations to assess the merits of LES of TC flow. The dynamic model also produces reasonable results within temporal averaging errors.

c_s	Nu_ω	Error (%)
DNS	22.53	–
0	23.80	5.7
0.05	23.32	3.5
0.1	22.32	0.9
0.1 (D')	22.15	1.71
0.2	19.96	11.4
0.3	18.93	16.0
0.4	19.05	15.6
0.6	14.71	34.4
Dynamic	21.96	2.5

Table 1. Nusselt number comparison for the simulations ran with $Rot = 0$, and the reference DNS case.

The LES models also improve the agreement of the azimuthal (streamwise) mean velocity profiles, shown in outer units for selected cases in Figure 1. Unless otherwise mentioned, the averaging is always done in the azimuthal and spanwise directions, as well as in time. The velocity in the bulk close to the outer cylinder is slightly lower, and this can be attributed to centrifugal stabilization.

Figure 2 shows the azimuthal (streamwise) mean velocity in inner units for both the inner and the outer cylinder. A reasonable collapse with the DNS reference is observed for the static model with $c_s = 0.1$ and for the dynamic model. The case with $c_s = 0.05$ lies slightly below the reference, while the case with $c_s = 0.2$ lies slightly above. This can be easily explained as the additional turbulent viscosity close to the wall suppresses turbulent mixing and delays the transition to the buffer and logarithmic layers at slightly higher values of r^+. The underresolved case (not shown here for the sake of conciseness) would lie below the $c_s = 0.05$. The data for the $c_s = 0.1$ case with the alternate van Driest model collapses onto that of the normal model case at the same c_s and is not shown. The profiles at the outer cylinder show a better match for a slightly lower value of c_s, due to the effect of centrifugal stabilization, but the differences are not substantial. This shows further proof that the LES self-adjusts when turbulent stresses are increased.

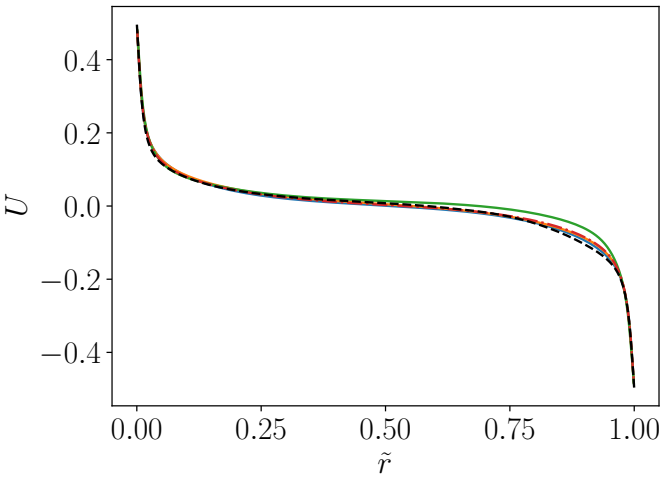

Figure 1. Mean azimuthal (streamwise) velocity profiles in outer units for selected cases including DNS reference for $Rot = 0$.

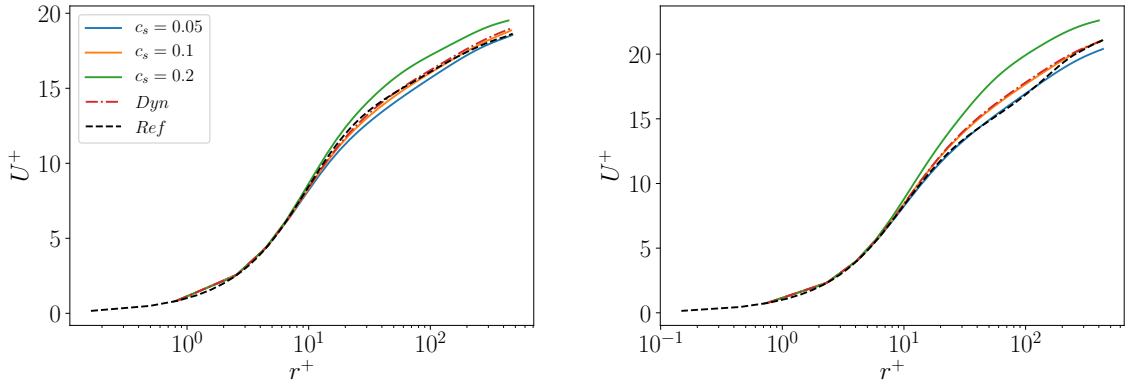

Figure 2. Mean azimuthal (streamwise) velocity profiles in wall units and for the inner cylinder (left) and outer cylinder (right) for selected cases including DNS reference for $Rot = 0$.

The effect of SGS models on the velocity fluctuations is shown in Figure 3, which shows the r.m.s. fluctuations for all three velocity components. From now on, we show only the inner cylinder as the profiles in the outer cylinder behave in a similar manner. The match between LES and the DNS reference is not as good as for the mean velocity, but could still be considered within acceptable realms. As expected, increasing c_s reduces the level of fluctuations due to the additional turbulent viscosity. The magnitude of the u'_θ peak is slightly higher for the LES models, while the u'_r fluctuations are clearly underestimated. This will later be shown to have an effect when $Rot \neq 0$. The axial (spanwise) velocity fluctuations also captured well.

These results show that for TC flow with $Rot = 0$, both the dynamic model and the static model with $c_s = 0.1$ (regardless of van Driest damping) show a reasonable match with the reference data. It could appear that the dynamic model produces no significant improvement over a static model with a calibrated constant, however, dynamic models are predictive while static models require calibration. We can directly look at the turbulent viscosity to explore

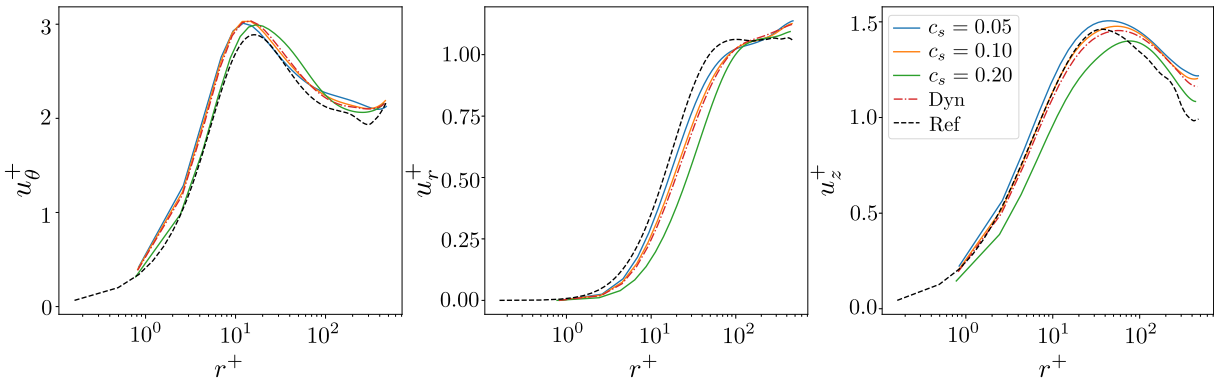

Figure 3. R.m.s. velocity fluctuation profiles in inner units for selected cases including DNS reference for $Rot = 0$.

the reasons for these effects. The left panel of Figure 4 shows the near-wall profiles of the averaged turbulent viscosity, while the other two panels show the axial and radial structure of the averaged turbulent viscosity for the static and dynamic models. The first thing to notice is that the D' simulation (with a van Driest model with $\alpha = 2$) only shows a difference for low values of r^+, where the turbulent viscosity is negligible with respect to the molecular viscosity. The value of α in $D(r)$ controls the asymptotic behavior of the turbulent viscosity ($\sim r^{+\alpha}$), but the values close to the wall are very small anyway for the grid resolution used, and thus the choice of damping model does not seem to matter.

The choice of c_s varies the turbulent viscosity by a constant factor and does not significantly change its spatial dependence. Both the static model with $c_s = 0.1$ and the dynamic model have similar effective turbulent viscosities, and both models capture the axial inhomogeneities of the flow: the footprint of the rolls can be clearly seen in the two right panels of Figure 4 which show the distribution of the azimuthally- and temporally-averaged turbulent viscosity. We note that both models only produce turbulent viscosities which are at most 30% of the molecular viscosity, and this could also explain the relatively small variance between the static and dynamic models.

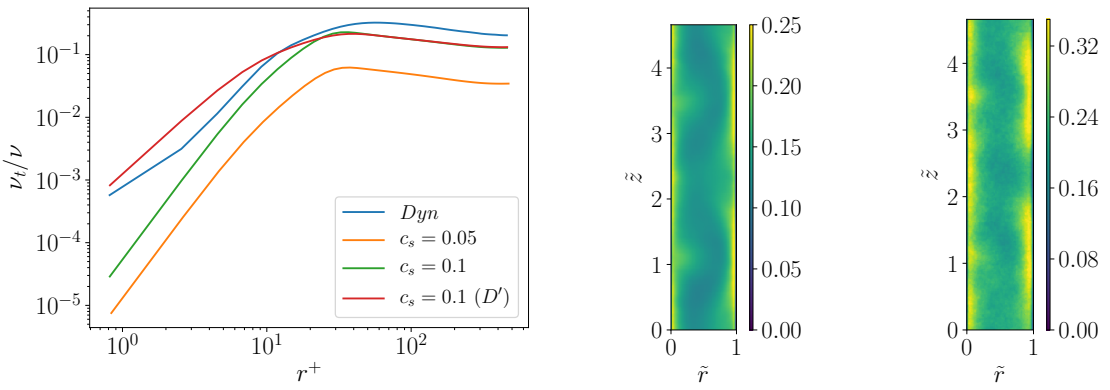

Figure 4. Left: Mean turbulent viscosity for selected cases. Middle and right: pseudocolor visualization of the azimuthally- and temporally averaged turbulent viscosity for the static model with $c_s = 0.1$ (middle) and the dynamic model (right).

4. The effect of mean rotation on Taylor-Couette LES

We now consider cases where mean rotation is present, i.e. $Rot \neq 0$. Table 2 shows the non-dimensional torque for the cases with rotation, including the reference datasets. Once again, the underresolved reference case ($c_s = 0$) overestimates the torque. The base errors are larger than in the previous case, where $Rot = 0$. Furthermore, with increasing c_s the results do not converge towards the resolved reference case. For $Rot = 0.0909$ (i.e. pure inner cylinder rotation), some improvement is seen, especially for $c_s = 0.2 - 0.3$, as the same trend of decreasing torque for increasing c_s is seen, but the error still remains around 8%, before increasing again for the "overdamped" cases. For $Rot = 0.3$ no significant decrease in the torque value is seen for any of the sub-grid stress models, as the LES model fails to self-adjust.

For the negative Rot case, significant reductions in Nu_ω are seen for all cases when compared to the cases with positive or zero Rot. Strong cyclonic rotation stabilizes the flow, and, if curved walls are present, it enhances the asymmetry between inner and outer boundary layers due to centrifugal effects. The torque is overestimated by the case with no SGS model and the static model with $c_s = 0.05$, while the static case with $c_s = 0.1$ and the dynamic model produce reasonably accurate results, similar to the $Rot = 0$ cases. For the "overdamped" cases, the torque is found to be smaller than the laminar torque, again indicating that increased stresses lead to decreased strains.

c_s	Nu_ω for $Rot = -0.0909$	Nu_ω for $Rot = 0.0909$	Nu_ω for $Rot = 0.3$
DNS	9.73	23.75	23.94
0	9.97	32.05	31.90
0.05	9.96	31.32	31.82
0.1	9.76	29.20	31.53
0.1 (D')	9.74	29.13	31.68
0.2	7.59	25.51	32.03
0.3	0.97	25.09	32.76
0.4	0.32	26.55	30.60
0.6	6.21	30.90	31.68
Dynamic	9.58	29.55	31.16

Table 2. Nusselt number comparison for the simulations ran with $Rot \neq 0$, and the reference DNS case.

The mean azimuthal (streamwise) velocity profiles also deviate substantially from the DNS references. Figure 5 shows these profiles at the inner cylinder for all Rot considered. For $Rot = -0.0909$, and small values of c_s, the velocity profiles have a weak dependence on c_s, and are close to the reference case. For $c_s = 0.3$ and $c_s = 0.4$, dispersive errors close to the wall cause anomalous torque measurements (measured by the wall-normal velocity gradient). A substantial amount of "wiggles" in the velocity field in the axial direction due to dispersive errors are also seen for the positive Rot cases. Dispersive errors appear to increase with increasing Rot. This will be revisited in a later section.

For $Rot = 0.0909$, large deviations are seen for the base case. Increasing c_s moves the curves towards the reference. For $c_s = 0.2$, which was found to produce the less erroneous torque, the deviations are smallest, even if they are still large on the graph. The deviations for $Rot = 0.3$ are even larger, and no improvement is seen modifying c_s. Neither the dynamic model nor any static model is able to correctly approximate the reference.

For now we focus on the cases with $Rot > 0$ to understand the deviations. Further indications of these deviations can be seen when looking at the velocity fluctuation profiles, shown in Figure 6. We only show $Rot = 0.3$ as it shows the largest deviations. The static model cases all seem to

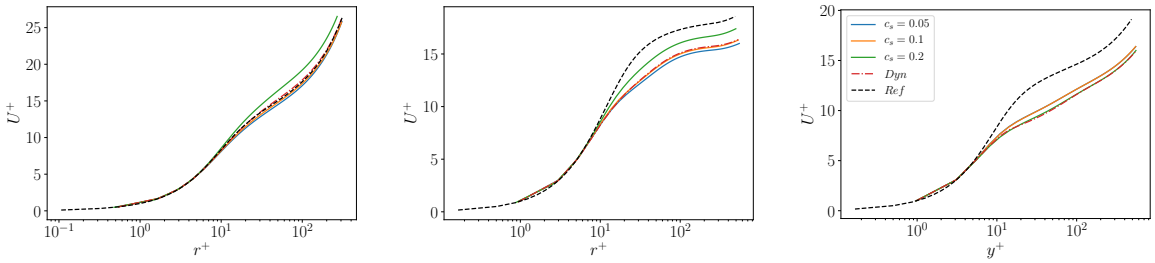

Figure 5. Averaged azimuthal (streamwise) velocity in inner units for (left) $Rot = -0.0909$, (middle) $Rot = 0.0909$ (pure IC rotation) and (right) $Rot = 0.3$ for selected cases including DNS reference.

overestimate the u'_θ (streamwise) velocity peak and locate it closer to the wall, while the dynamic case captures better its magnitude. The inverse happens for the u'_r (wall-normal) fluctuation profile, which is underestimated by all cases, and most considerably by the dynamic model. For the u'_z (spanwise) fluctuations, the static model captures the behaviour reasonably well for the low c_s while the dynamic model again underestimates the fluctuations.

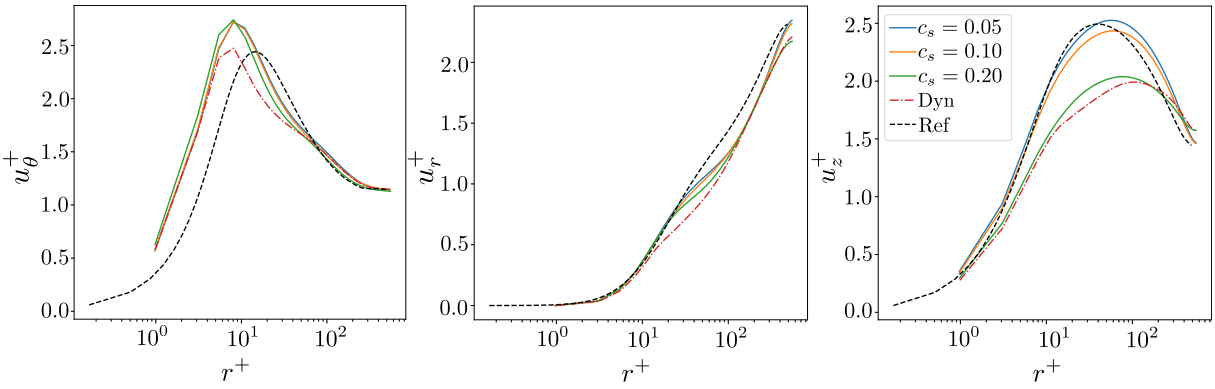

Figure 6. R.m.s. profiles of the velocity fluctuations for $Rot = 0.3$ for selected cases including DNS reference.

We can elucidate the reasons for the failure of the sub-grid stress models by looking at the turbulent viscosity. The left panel of Figure 7 shows the turbulent viscosity for the static model with $c_s = 0.1$, while the right panel shows the turbulent viscosity for the dynamic model. All static models produce a relatively similar turbulent viscosity regardless of Rot, and the cyclonic rotation tends to slightly decrease ν_t due to the smaller strains. For the static model, only the strain can change the turbulent viscosity, as the mixing length ($c_s^2\Delta^2$) is kept constant. The averaged strain rate $|\mathcal{S}|$ is shown in the left panel of figure 8, and indeed it appears to be relatively independent of background rotation for $Rot \geq 0$. Therefore, this does not seem to be adequate to reproduce the dependence of the mean velocity profiles on Rot.

The dynamic model does show a dramatic increase for ν_τ for $Rot = 0.3$, explaining why the velocity fluctuations for the dynamic model seen in 6 were much smaller than those for the static case. This adequately corrects for the magnitude of the peak of u'_θ, but this also substantially constrains the radial velocity fluctuations, leading to their underestimation as seen in figure 6. The ordering of the curves is different with respect to the static model, and here the cyclonic case has the lowest turbulent viscosity, which is in line with what we expect from the smaller reference torques.

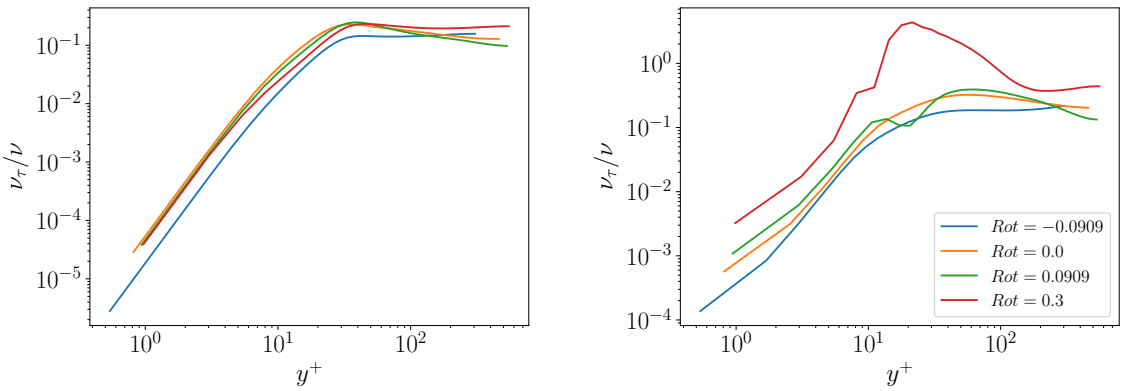

Figure 7. Turbulent viscosity for the static case with $c_s = 0.1$ (left) and the dynamic case (right) for the four rotation parameters.

The right panel of figure 8 shows the variations of the mixing length for the reference cases. This is a Reynolds averaged-like mixing length for the mean azimuthal velocity profile given by:

$$l_m = \frac{r_i u_\tau}{r^2} \left(\frac{\partial (U_\theta / r)}{\partial r} \right). \tag{3}$$

While this mixing length is a RANS-type mixing length resulting from a complete averaging of fluctuations, and thus cannot be directly compared to the LES mixing length, it can give an indication of why the LES subgrid models fail in rotating flows. The right panel of figure 8 shows a strong variation of the mixing length of almost of an order of magnitude, caused by the background anti-cyclonic rotation. The inset shows a zoom-in of the near-wall region, with the mixing length compensated so the differences can be clearly seen.

The mixing length is a proxy for fluctuations, both for the total fluctuations in the reference case and for the SGS fluctuations in the LES. The enhanced SGS fluctuations, modeled in the static LES by the constant mixing length $c_s^2 \Delta^2$ multiplied by the average strain $|\mathcal{S}|$ rate are not captured. The average strain, the only varying term in the turbulent viscosity equation, remains approximately the same in the near-wall region.

However, the dynamic model also fails. The dynamic model can reproduce aspects of the rotating flow, as the enhanced mixing length (cf. figure 7*b)*), but still yields unsatisfactory results. This is because the turbulent viscosity approximation assumes a degree of isotropy, but there is a clear anisotropy in the fluctuations, enhanced by rotation. The SGS cannot be adequately represented by an isotropic molecular viscosity. The stress-strain correlation, which is already low without rotation, could potentially be even worse with anti-cyclonic rotation: the failure of the LES models to decrease torque (strain) also points in this direction.

This is evident in the gross underestimation of radial and streamwise fluctuations in Figure 6 by the dynamic model. The two different directions of rotation act in opposite ways on the SGS. As cyclonic rotation tends to reduce the level of overall fluctuations, the SGS models become less important, and it can be seen that even the case with no SGS model has a small error for Nu_ω for $Rot = -0.0909$, but a large error for $Rot = 0.0909$. This reduced level of fluctuations can also be seen by the small mixing length of figure 8.

To show evidence of the anisotropy of the SGS, we filter a single DNS reference snapshot using a box-filter, by downsampling the resolution by a factor two in every direction. We then compute the values of the SGS for the single snapshot. Figure 9 shows two of these stresses: the radial and axial stresses of the azimuthal velocity. Aside from the saw-tooth oscillations of the

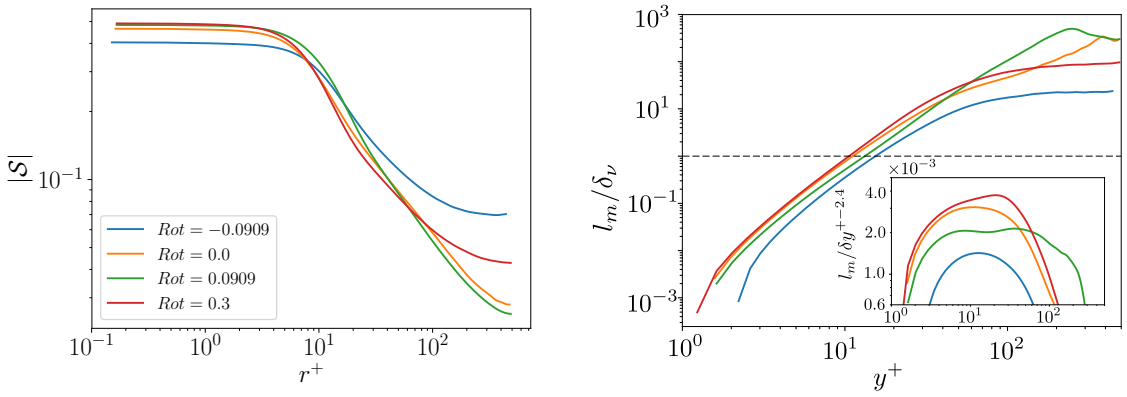

Figure 8. Left: Average strain rate for the reference cases and the three values of *Rot*. Right: mixing length for reference cases. Dashed line shows $l_m/\delta_\nu = 1$, separating the regions where the molecular viscosity is either larger or smaller than the equivalent turbulent viscosity. The inset shows a compensated l_m/δ_ν highlighting the variation with *Rot*.

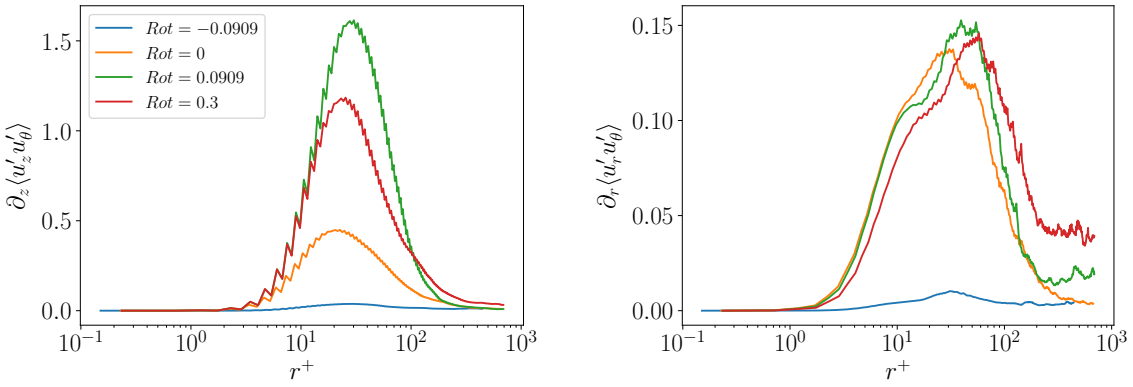

Figure 9. Two components of the SGS for all rotation ratios. The degree of anisotropy increases with increasing rotation.

graphs, due to the discrete nature of the box-size filter, two things can be noticed here: firstly, the $Rot = -0.0909$ case has extremely small SGS values, even if the average strain was seen in the left panel of 8 to be comparable to the other cases. This could explain the low values of Nu_ω seen for high c_s. Secondly, the values for the radial SGS in the azimuthal velocity are more or less constant with increasing *Rot*, but the values of the axial SGS depend substantially on *Rot*, and are almost five times larger for $Rot = 0.3$ than for the case with no rotation. Together, these graphs show that indeed, the anisotropy of the SGS increases with rotation. This provide a rationale for the failure of the LES, and also the high dispersive errors in the axial direction seen for anti-cyclonic rotation.

For completeness, we explore the effect of removing the mean Coriolis force and applying the rotation directly as a boundary condition. In principle, this reformulates the sub-grid Coriolis force fluctuations, a possible source of discrepancy, as part of the non-linear term. However, simulations in an inertial frame also incur in additional losses of accuracy. It has been shown that finite-differences are not Gallilean invariant, and that dispersive errors for second order

finite differences are smallest when the mean velocity is close to zero [23]. Thus, by running in the inertial frame we amplify dispersive errors.

To check the balance of effects, we ran two additional cases for pure inner cylinder rotation in an inertial frame both with either a static Smagorinsky model and damping constants $c_s = 0.05$ and $c_s = 0.1$, as well as an underresolved reference case with no sub-grid model. The Nusselt numbers for the inertial frame and the convective frame cases are compared in Table 3. These can be benchmarked against the reference $Nu_\omega = 23.5$. In both cases, the errors are large, but we note that they are larger for the inertial frame as the increased dispersive errors dominates any possible effect which could have come from reformulating the Coriolis forces. Finally, we mention that preliminary results have shown that the axial (spanwise) resolution is especially critical for obtaining accurate results: this direction shows the highest dispersion in the velocity fields, especially for the large *Rot* cases.

c_s	Nu_ω (Convective frame)	Nu_ω (Inertial frame)
0.	32.1	34.0
0.05	31.3	33.2
0.1	29.4	31.1

Table 3. Nusselt number comparison for pure inner cylinder rotation in both convective and inertial reference frames.

5. Summary and outlook

In this report we have shown the possibility of using large eddy simulations to obtain reasonable results for Taylor-Couette flow at resolutions below what would be considered well resolved for a direct numerical simulation. LES was found to give good estimates of not only the torque and mean velocity profiles but also the fluctuations for cases with no mean rotation. Increasing anti-cyclonic rotation destroys the validity of the LES sub-grid models, as the linear relationship between sub-grid fluctuations and strain of the static model, as well as the isotropic turbulent viscosity hypothesis of both static and dynamic models come into question. The SGS models tend to severely underestimate the torque increases caused by anticyclonic rotation. The LES of cyclonic rotation is more accurate when compared to the DNS reference, as this rotation stabilizes the flow, and overall reduces the fluctuation level, so is less demanding on SGS models.

However, the main sources of discrepancy occur close to the wall, and could potentially not affect the behaviour of the large-scale motions, i.e. the Taylor rolls far from the wall. Therefore, overdamped simulations of Taylor-Couette flow which reveal the underlying large-scale structure appear to be possible.

In Figure 10 we show visualizations of the flow at the mid-gap, for both the resolved reference DNS (at a reduced domain) and the "overdamped" LES with the static model and $c_s = 0.6$ for three of the four values of *Rot* simulated. The figure shows that the underlying axial signatures of the large-scale motion are preserved at the mid-gap if they exist for the reference case. For $Rot = 0.0909$ where the signature is the strongest, the overdamped LES also preserves a very clear axially-pinned and quasi-axisymmetric structure, with certain spaced out blobs that could correspond to the wavyness found in Ref. [14].

For $Rot = 0$, the large-scale motion shows a larger degree of azimuthal fluctuations, which are captured by the overdamped LES. For the largest *Rot* simulated, no predominant large-scale motion is seen both in the reference case and in the overdamped LES. Overdamped LES appears to be a promising tool for rapidly exploring the parameter space to determine where axially pinned large-scale rolls are found in a faster manner than DNS.

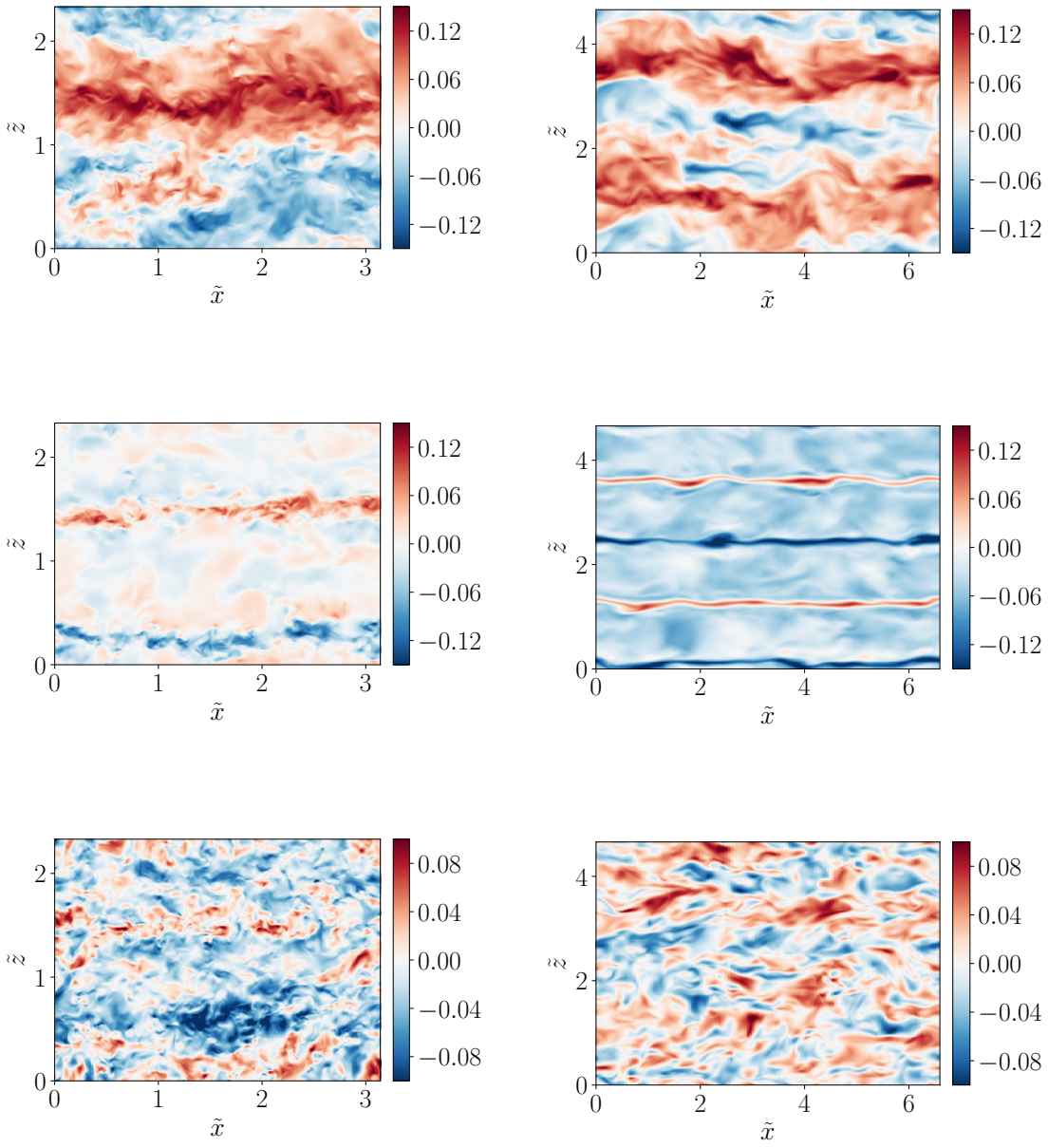

Figure 10. Pseudocolor visualization of u_θ at the mid-gap for the reference DNS cases (left) and the LES cases with the static model and $c_s = 0.6$ (right) for the three rotation numbers $Rot = 0$ (top), $Rot = 0.0909$ (middle) and $Rot = 0.3$ (bottom). The DNS domains are half the length in both spanwise and streamwise directions. The streamwise coordinate $\tilde{x}$ is defined as $\tilde{x} = r\theta/d$.

By this, we note that overdamped LES can reproduce some features of the large-scale motions seen in the mid-gap, and can be a useful tool for a fast exploration of the TC parameter space to check for the presence of axially pinned large-scale structures.

Acknowledgments
We thank the participants of the Third Madrid Turbulence Workshop, and especially T. Kwon and D. Feldmann for their comments on the manuscript. We also thank R. J. A. M. Stevens for valuable discussions. Funded in part by the Coturb program of the European Research Council. We also gratefully acknowledge computational time for the simulations provided by SURFsara on resource Cartesius through a NWO grant.

References

[1] Moin P and Kim J 1982 *J. Fluid Mech.* **118** 341–377
[2] Rütten F, Schröder W and Meinke M 2005 *Phys. Fluids* **17** 035107
[3] Kosovic B 1997 *J. Fluid Mech.* **336** 151–182
[4] Sagaut P 1998 *Large Eddy Simulation for incompressible flows: An Introduction* (Berlin: Elsevier)
[5] Meneveau C and Katz J 2000 *Ann. Rev. Fluid Mech.* **32** 1–32
[6] Grossmann S, Lohse D and Sun C 2016 *Ann. Rev. Fluid Mech.* **48** 53–80
[7] Huisman S G, Scharnowski S, Cierpka C, Kähler C, Lohse D and Sun C 2013 *Phys. Rev. Lett.* **110** 264501
[8] Ostilla-Mónico R, Verzicco R, Grossmann S and Lohse D 2016 *J. Fluid Mech.* **768** 95–117
[9] Spandan V A, Ostilla-Mónico R, Lohse D and Verzicco R 2016 *J. Phys: Conf. Series* **708** 012006
[10] Hwang Y and Cossu C 2010 *Phys. Rev. Lett.* **105** 044505
[11] Hwang Y and Cossu C 2011 *Phys. Fluids* **23** 061702
[12] Smits A J, McKeon B J and Marusic I 2011 *Ann. Rev. Fluid. Mech.* **43** 353–375
[13] Andereck C D, Liu S S and Swinney H L 1986 *J. Fluid Mech.* **164** 155–183
[14] Ostilla-Mónico R, Verzicco R and Lohse D 2015 *Phys. Fluids* **27** 025110
[15] Verzicco R and Orlandi P 1996 *J. Comput. Phys.* **123** 402–413
[16] van der Poel E P, Ostilla-Monico R, Donners J and Verzicco R 2015 *Comput. Fluids* **116** 10–16
[17] Singh H, Suazo C A T and Liné A 2016 *Phys. Rev. E* **94** 053120
[18] Germano M, Piomelli U, Moin P and Cabot W H 1991 *Phys. Fluids A* **3** 1760–65
[19] Piomelli U and Liu J 1994 *AGARD Conf. Proc.* **551** 3
[20] Haertel C and Kleiser L 1998 *J. Fluid Mech.* **356** 327–352
[21] Ostilla-Mónico R, Lohse D and Verzicco R 2016 *Phys. Rev. Flu.* **1** 054402
[22] Jiménez J and Moser R D 2000 *AIAA J.* **38** 605–612
[23] Bernardini M, Pirozzoli S, Quadrio M and Orlandi P 2013 *J. Comput. Phys.* **232** 1–6